

Paracrine WNT5A Signaling Inhibits Expansion of Tumor-Initiating Cells

Nicholas Borcharding^{1,2}, David Kusner^{1,3}, Ryan Kolb^{1,4}, Qing Xie^{1,5}, Wei Li¹, Fang Yuan^{1,6}, Gabriel Velez², Ryan Askeland¹, Ronald J. Weigel^{7,8}, and Weizhou Zhang^{1,2,3,4,8}

Abstract

It is not well understood how paracrine communication between basal and luminal cell populations in the mammary gland affects tumorigenesis. During ErbB2-induced mammary tumorigenesis, enriched mammary stem cells that represent a subpopulation of basal cells exhibit enhanced tumorigenic capacity compared with the corresponding luminal progenitors. Transcript profiling of tumors derived from basal and luminal tumor-initiating cells (TIC) revealed preferential loss of the noncanonical Wnt ligand WNT5A in basal TIC-derived tumors. Heterozygous loss of *WNT5A* was correlated with shorter survival of breast cancer patients. In a mouse model of ErbB2-induced breast cancer,

Wnt5a heterozygosity promoted tumor multiplicity and pulmonary metastasis. As a TGF β substrate, luminal cell-produced WNT5A induced a feed-forward loop to activate SMAD2 in a RYK and TGF β R1-dependent manner to limit the expansion of basal TIC in a paracrine fashion, a potential explanation for the suppressive effect of WNT5A in mammary tumorigenesis. Our results identify the WNT5A/RYK module as a spatial regulator of the TGF β -SMAD signaling pathway in the context of mammary gland development and carcinogenesis, offering a new perspective on tumor suppression provided by basal-luminal cross-talk in normal mammary tissue. *Cancer Res*; 75(10); 1972–82. ©2015 AACR.

Introduction

The canonical Wnt pathway activates β -catenin and is integral in regulating self-renewal of normal stem cells, and the subversion of the canonical Wnt signaling has been implicated in tumorigenesis (1). In contrast, noncanonical Wnt signaling is characterized by a lack of requirement for β -catenin and has been studied for its role in embryonic patterning, gastrulation, and organogenesis (2–6). Moreover, noncanonical Wnt is proposed to antagonize canonical signaling (7). WNT5A is the archetype of noncanonical Wnt ligand and has both tumor-suppressive and tumor-promoting effects. WNT5A is tumor suppressive in acute

myelogenous leukemia (8), colorectal cancer (9), breast cancer (10), and ovarian carcinoma (11), whereas WNT5A increases aggressiveness in various cancers (6). In breast cancer, contradictory results have been reported about the expression of WNT5A in breast cancer based on different methods (12–14). Jönsson and colleagues (13) found the decrease in WNT5A expression through cancer progression (14). WNT5A expression in the developing murine gland is highest in terminal end buds where loss of TGF β signaling correlates with the decrease of WNT5A; in turn, WNT5A mediates the suppressive effect of TGF β during mammary gland development (15). Inhibition of the TGF β signaling pathway by DNIR, a dominant-negative mutation TGF β receptor 2 (TGF β R2), led to increased tumor growth and decreased WNT5A expression (10), a similar phenotype as genetic deletion of WNT5A (15), suggesting that WNT5A is a TGF β -downstream effector and mediates the tumor-suppressive effect of TGF β .

Several major noncanonical receptors for WNT5A have been studied in development and cancer, including RYK, Ror1/2, and Fzd4 (16–18). RYK is a divergent receptor tyrosine kinase (RTK) with a shortened extracellular Wnt-inhibitory factor domain (19). Because of unusual substitutions in the kinase domain, RYK has an inactive kinase domain and sequesters Wnt ligands from interacting with other receptors (19). Increased expression of RYK has been linked to poor outcomes in ovarian cancer (20). RTK-like orphan receptors (ROR) have been studied for their role in embryonic patterning, musculoskeletal, and neuronal development (21). ROR1 and ROR2 have growing evidence for their role in the progression of malignancies (18, 21).

Our findings demonstrate a novel regulatory mechanism for the TGF β -SMAD signaling pathway via WNT5A. The induction of SMAD2 phosphorylation and activation by WNT5A depends on TGF β R1 kinase activity and RYK. These findings add an avenue to understand the complex environment during mammary tumorigenesis.

¹Department of Pathology, University of Iowa, College of Medicine, Iowa City, Iowa. ²Medical Science Training Program, University of Iowa, College of Medicine, Iowa City, Iowa. ³Molecular and Cellular Biology Program, University of Iowa, College of Medicine, Iowa City, Iowa. ⁴Immunology Program, University of Iowa, College of Medicine, Iowa City, Iowa. ⁵College of Veterinary Medicine, Nanjing Agricultural University, Nanjing, P.R. China. ⁶Department of Nephrology, The Second Xiangya Hospital, Central South University, Changsha, Hunan, P.R. China. ⁷Department of Surgery, University of Iowa, College of Medicine, Iowa City, Iowa. ⁸Holden Comprehensive Cancer Center, University of Iowa, College of Medicine, Iowa City, Iowa.

Note: Supplementary data for this article are available at Cancer Research Online (<http://cancerres.aacrjournals.org/>).

N. Borcharding, D. Kusner, and R. Kolb contributed equally to this article.

Current address for R. Askeland: University of South Dakota Sanford School of Medicine, Sioux Falls, SD.

Corresponding Author: Weizhou Zhang, University of Iowa, 200 Hawkins Drive, Iowa City, IA 52242. Phone: 319-335-8214; Fax: 319-335-8453; E-mail: weizhou-zhang@uiowa.edu

doi: 10.1158/0008-5472.CAN-14-2761

©2015 American Association for Cancer Research.

Materials and Methods

Mouse illumina array

Tumors were generated from our previous study (22). RNAs were isolated from tumors (QIAGEN) and their quality was assessed. RNA was submitted to the Genomics Division of the University of Iowa for microarray analysis. Microarray data (GEO accession number: GSE64487) were normalized and transformed into \log_2 expression. Transcriptome heatmap and the heatmap for differentially expressed genes were generated in R using the gplots package. The volcano plot was made in R using the ggplot2 package. Fold change was found by the average \log_2 expression difference in paired basal tumor-initiating cell (TIC) and luminal TIC tumors. Genes highlighted in the volcano plot have a P value of <0.05 and an average \log_2 change ≥ 1.58 (equal to linear 3.0-fold change).

The Cancer Genome Atlas data analyses

The UCSC Cancer Genome Browser (<https://genome-cancer.ucsc.edu>) was used to assess copy-number variations (CNV) across all available cancer datasets in The Cancer Genome Atlas (TCGA; ref. 23). Level 3 Illumina HiSeq 2000 RNAseq for TCGA breast cancer cohort was used. RNAseq expression data were transformed as $\log_2(x + 1)$. Differences in sample numbers between figures were a result of sorting by categorical data.

Immunohistochemistry

Paraffin embedded tissues were deparaffinized and antigens were retrieved with Antigen Unmasking Solution (Vector Laboratories) or with S1700 (Dako). WNT5A antibody (Genetex) was used at a 1:200 dilution. We consulted with Dr. Ryan Askeland who is a clinical pathologist and defined the intensity of WNT5A staining. The staining intensity of WNT5A was given a scoring system as 0, 1+, 2+, and 3+. For example, we defined the strongest signal as 3+ (an example would be the Fig. 3A, adjacent normal tissues) and the signals equivalent to IgG nonimmune antibody control as 0. We combined 0 and 1+ as low, 2+ as medium, and 3+ as high.

Separation of mammary epithelial cells and spheroid growth in Matrigel

We followed previously established protocols (24) and also included the detailed protocol in Supplementary Methods. Briefly, mammary glands were sequentially digested. Single cells were labeled with a cocktail of antibodies for flow cytometry to separate different epithelial cells. For spheroid growth on Matrigel (BD Biosciences), 1,000 cells were seeded onto Matrigel-coated 8-well chamber slide (24). Spheroids were photographed 3 weeks later as before (22) and the size was quantitated (25).

Cells

HMLE cells (provided by Dr. Jing Yang, University of California, San Diego, San Diego, CA) and MCF10A cells (purchased from the ATCC) were maintained using 10% FBS-containing F12 media (Life Technologies) supplemented with insulin (10 $\mu\text{g}/\text{mL}$), hydrocortisone (2 $\mu\text{g}/\text{mL}$), and EGF (10 ng/mL). For both cell lines, we constantly monitored their morphology, confirmed their epithelial cell feature by positive cytokeratin 5 or 8 staining, and further confirmed their identity with three-dimensional spheroid growth. Primary mammary epithelial cells,

including basal and luminal mammary epithelial cells, were cultured using EpiCult-B medium (StemCell).

shRNA and siRNA

cDNAs of two-independent shRNAs for RYK were constructed into lentiviral vector pLSLPw-GFP with targeting sequences: shRNA-1: 5'-GC ACA TTT GTC TTC CAG AA-3'; shRNA-2: 5'-CC TGT ACT GGC AAA GTA GA-3'. Viral particles were packaged, following by infection of MCF10A cells and purification of GFP-positive cells using flow cytometry (26). siRNAs for TGF β R1 (siCON, si-1, and si-3 used in Fig. 6B, no targeting information released) were purchased (Sigma-Aldrich).

Cell lysates, immunoprecipitation, immunoblots, and antibodies

Cells were lysed in cell lysis buffer (50 mmol/L Tris-HCl pH7.5, 1 mmol/L EDTA, 1 mmol/L EGTA, 1% Triton X-100, 100 mmol/L KCl, 50 mmol/L NaF, 10 mmol/L Na₂-glycerophosphate, 1 mmol/L Na₃VO₄, and supplemented with protease inhibitor set; Roche). For immunoprecipitation, 1 mg cell lysate was used to incubate with 1 $\mu\text{g}/\text{mL}$ of antibodies. Immunocomplex was precipitated using protein A/G sepharose (Thermo Fisher Scientific). Antibodies used are as follows: anti-p-SMAD2/3, anti-p-JNK1/2, and anti-TGF β R1 (Cell Signaling Technology); anti-SMAD1/2/3, anti-JNK1/2, and anti-RYK antibodies (Santa Cruz Biotechnologies); anti-WNT5A (Genetex); and anti- α -tubulin (Sigma-Aldrich); anti-keratin 8 (clone TROMA-I, Developmental Studies Hybridoma Bank at the University of Iowa, Iowa City, IA).

Murine models

All mice were maintained according to the University of Iowa Institutional Animal Care and Use Committee guidelines. *Wnt5a*^{fl/fl} mice in the C57BL/6 background were kindly provided by Dr. Terry Yamaguchi (National Cancer Institute; ref. 27). *MMTV-ErbB2* mice in the FVB/N genetic background [FVB/N-Tg (*MMTVneu*)202Mul/J]; ref. 28] were crossed with *Wnt5a*^{+/-} mice (B6;129S7-*Wnt5a*^{tm1Amc}/J) in the C57BL/6 background (The Jackson Laboratory; ref. 29). F1 generations of *MMTV-ErbB2/Wnt5a*^{+/+} and *MMTV-ErbB2/Wnt5a*^{+/-} mice were used to isolate mammary epithelial cells and tumorigenesis studies. Tumor onset date was recorded and mice were euthanized when largest tumor reached 2 cm in diameter. Lung metastasis was determined by hematoxylin and eosin (H&E) staining.

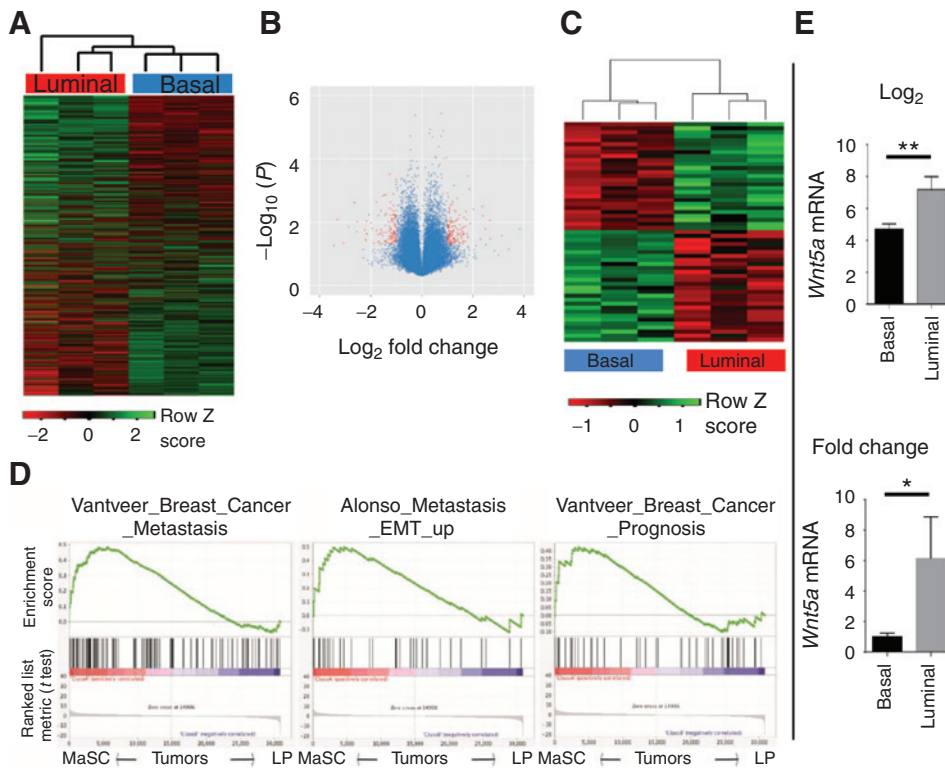
Statistical analysis and data presentation

Data are presented as mean \pm SEM for most studies or mean values \pm 95% confidence interval (CI) for genomic data. Microarray data are reported as \log_2 . TCGA RNAseq data are reported in $\log_2(x + 1)$. The Welch T test was used for genomic results. The Student T test was used for the remaining experiments. The Mantel-Cox log-rank test was used for survival curve analysis (Prism v6; GraphPad). Gene expression of human mammary gland cell populations used GEO37223 using normalized expression (30).

Results

Transcriptome comparison between ErbB2-induced tumors from different TICs

Our previous work has demonstrated a variance in tumorigenic capacity in different mammary epithelial populations of

**Figure 1.**

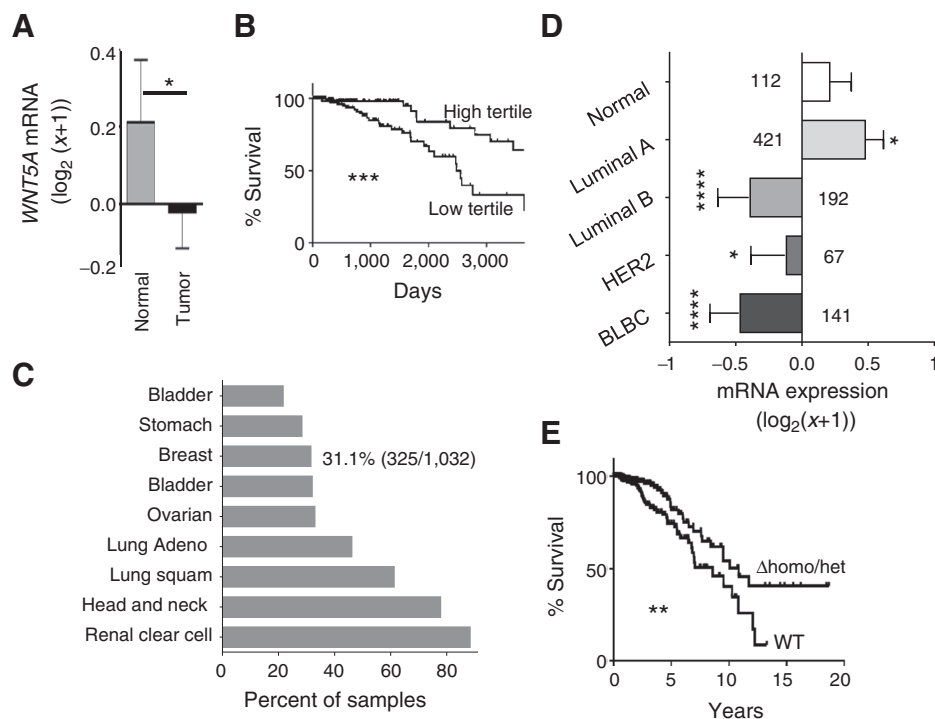
Transcriptome comparison between basal TIC and luminal TIC tumors. A, heatmap for unsupervised clustering of gene profiles from paired tumors derived from basal TICs (basal, red) and luminal TICs (luminal, blue). The whole transcriptomes were clustered using R gplots; $n = 3$ per group. B, the volcano plot showing differentially expressed between luminal and basal TIC tumors, with a P value of <0.05 and \log_2 fold change >1.58 (linear 3-fold change) highlighted in red. C, 55 genes were identified to fit the criteria in B, with exclusive expression in basal TIC- and luminal TIC-derived tumors. D, GSEA was used to analyze the difference of biologic signaling pathways between basal TIC- or luminal TIC-formed tumors based transcriptome data from A. Basal TIC tumors upregulate signaling pathways related to breast cancer metastasis and bad prognosis. Nominal P values <0.001 for pathways mentioned. E, *WNT5A* expression in mouse basal TIC and luminal TIC tumors. Both \log_2 values (top) and linear fold change (bottom) are shown. *, $P = 0.019$; **, $P = 0.0076$; $n = 3$.

MMTV-ErbB2 mice (22). $CD24^{\text{med}}CD49^{\text{hi}}$ basal cells (basal TIC) gave rise to larger tumors at a greater incidence than $CD24^{\text{hi}}CD49^{\text{lo}}CD61^+$ luminal progenitors (luminal TIC). We performed transcript profiling using three-paired tumor samples, with each pair of basal TIC-, or luminal TIC-formed tumors from the contralateral inguinal mammary glands of the same mouse to minimize differences from the recipient mouse. Basal TIC tumors were clustered together with similar gene-expression pattern and separated from luminal TIC tumors (Fig. 1A). We used a threshold of 3-fold change (\log_2 change 1.58) and a P value of less than or equal to 0.05, and found 55 genes meeting the criterion as shown in the volcano plot (Fig. 1B). Among these genes, we found 28 upregulated and 27 downregulated genes in basal TIC tumors when compared with their paired luminal TIC tumors (Supplementary Table S1; Fig. 1C). We validated the array dataset by real-time PCR using a panel of 13 upregulated genes (Supplementary Fig. S1A) and 11 downregulated genes (Supplementary Fig. S1B) in basal TIC tumors and nearly all examined genes exhibited similar patterns. We searched the literature and found many genes with known function in cancer (Supplementary Table S1). Gene Set Enrichment Analysis (GSEA; ref. 31), a computational method that determines whether a defined set of genes show concordant differences between biologic states, revealed that eight pathways related to cell-cycle progression, five pathways related to RNA/Protein synthesis and processing, and three pathways related to metastasis and poor prognosis were upregulated in basal TIC tumors (Fig. 1D, other pathways not shown). These data suggest that basal TIC tumors have more aggressive gene signature than luminal TIC tumors.

Wnt5a is lost in more aggressive mouse basal TIC tumors and human breast cancer

In particular, we found *Wnt5a* to be nearly 6-fold (\log_2 difference: 2.534) downregulated in basal TIC mouse tumors compared with luminal TIC tumors (Supplementary Table S1; Fig. 1E). We identified a similar *WNT5A* decrease in human breast cancer samples relative to normal tissues in the breast cancer dataset deposited by TCGA (Fig. 2A). Lower *WNT5A* mRNA in breast cancer was significantly correlated with shorter patient survival (Fig. 2B). Examining the 58 probes of the Infinium HumanMethylation450 methylation data for *WNT5A* within the TCGA breast cancer, we found no significant correlation between *WNT5A* expression and DNA methylation (Supplementary Fig. S2A). Rather, we found that mono- or biallelic loss of *WNT5A* occurs in 31.1% within the breast cancer dataset and greater than 20% of samples in eight other cancers from TCGA (Fig. 2C). Loss of *WNT5A* was seen in more aggressive subtypes, where 60% of basal-like breast cancer (BLBC), 51% of HER2-positive, and 38% of luminal B have allelic loss, only 18% have allelic loss in the luminal A subtype (Supplementary Table S2). The mono- or biallelic loss of *WNT5A* in breast cancer samples led to decreased *WNT5A* expression in tumor stages II–IV of breast cancer, but not in stage I (Supplementary Fig. S2B). Lower *WNT5A* mRNA expression was also seen in more aggressive breast cancer subtypes, including luminal B, HER2, and basal-like relative to normal and luminal A subtype (Fig. 2D). In addition, we found that patients with loss of one *WNT5A*-allele possessed significantly shorter overall survival (OS) than patients with *WNT5A*-bialleles (Fig. 2E).

We observed strong staining of *WNT5A* at the normal mammary ducts and acini by IHC (Fig. 3A). Low *WNT5A* expression

**Figure 2.**

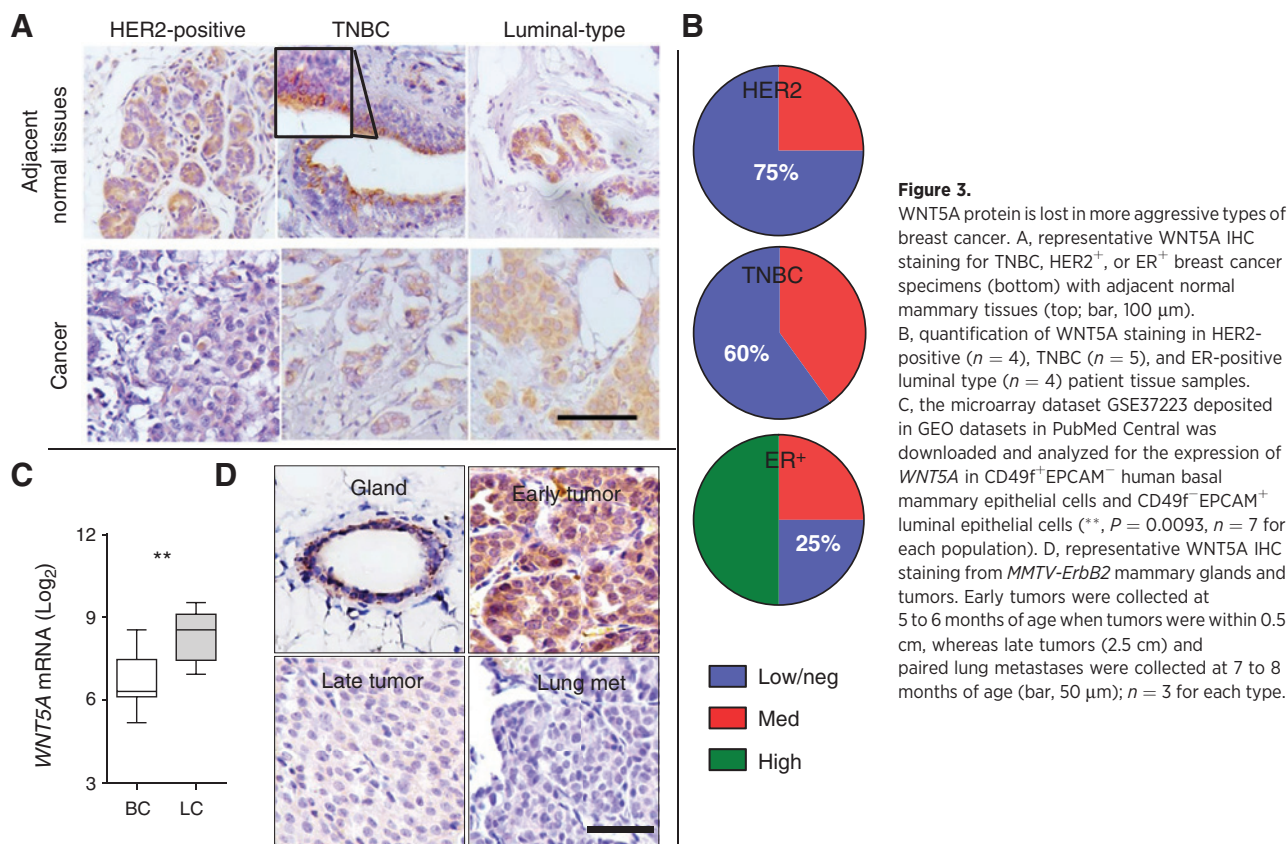
Heterozygous loss of *WNT5A* is common in cancer. A, *WNT5A* expression in TCGA Illumina HiSeq level 3 breast cancer dataset by sample type (*, $P = 0.0154$; $n = 112$ for normal tissues and $n = 1,040$ for invasive cancer). B, Kaplan-Meier curve to show the OS between the highest *WNT5A*-expressing samples ($n = 126$) and the lowest *WNT5A*-expressing samples ($n = 125$) among the Agilent G4502A level 3 microarray TCGA breast cancer dataset; ***, $P = 0.0003$. C, CNVs from different TCGA datasets were analyzed using UCSC Cancer Genome Browser and plotted as percentages of specimens with any loss of *WNT5A* alleles. D, *WNT5A* expression in breast cancer TCGA Illumina HiSeq level 3 by PAM50 molecular subtype. P values comparing normal samples ($n = 60$) to luminal A ($n = 211$; *, $P = 0.0142$), luminal B ($n = 128$; ****, $P < 0.0001$), HER2 ($n = 58$; *, $P = 0.0389$), and BLBC ($n = 78$; ****, $P < 0.0001$). E, Kaplan-Meier curve to show the OS between *WNT5A* bialleles (WT; $n = 519$) and either homozygous or heterozygous deletion of *WNT5A* alleles (Δ homo/het, $n = 249$) among Illumina HiSeq RNAseq level 3 breast cancer data; **, $P = 0.0098$.

was seen in 75% and 60% of samples of triple-negative breast cancer (TNBC) and HER2 subtypes, respectively (Fig. 3B). In contrast, 75% of estrogen receptor (ER)⁺ possessed moderate to high *WNT5A* staining (Fig. 3A and B). We noticed a clear luminal distribution of *WNT5A* in normal mammary ducts (Fig. 3A). We downloaded GEO dataset GSE37223 (30) and found human luminal cells had approximately 3-fold increase (\log_2 difference: 1.733) in *WNT5A* mRNA relative to basal epithelial cells (Fig. 3C). We found a similar luminal *WNT5A* staining in mouse mammary ducts (Fig. 3D, gland). Consistent with *WNT5A* loss in human breast cancer, *WNT5A* expression was evident in preneoplastic mammary gland and early tumors (less than 0.5 cm in diameter with evident features of ductal carcinoma *in situ* (DCIS; Fig. 3D, gland and early tumor) and was decreased in late-stage tumors (2 cm in diameter) and lung metastasis (Fig. 3D), in agreement with its tumor-suppressive role (10).

WNT5A suppresses the growth of basal TIC via a paracrine fashion

WNT5A is known to suppress breast cancer (10), whereas it is largely unknown how *WNT5A* inhibits tumorigenesis. We hypothesize that *WNT5A* is a potential niche component from luminal epithelial cells to suppress basal TIC expansion, counterbalancing the canonical Wnt ligand in promoting the expansion of basal cells (32, 33). We used our established scheme (Supple-

mentary Fig. S3) and isolated lineage⁻CD24⁺CD49f^{high} basal TIC and lineage⁻CD24^{high}CD49f^{low}CD61⁺ luminal TIC from preneoplastic mammary gland of 5-month-old *MMTV-ErbB2* female mice (22). We grew them under mammosphere medium to assay the expansion of mammary stem cells or progenitors with or without *WNT5A* (34). After 1-week incubation, untreated cells had an average of 42.3 spheres per well, whereas *WNT5A*-treated cells had an average of 11.7 spheres (Supplementary Fig. S4A and S4B). The suspension mammosphere culture system generated significant amount of cell aggregates. Similar phenomenon was noticed in other studies and reviewed (35). We chose to use a well-established Matrigel-based system to grow spheroids as a more relevant *ex vivo* tumor model (24, 36). Different doses of *WNT5A* treatment did not significantly alter the spheroid number from basal TICs (Supplementary Fig. S4C), but significantly reduced the spheroid size from basal TICs not from luminal TICs (Fig. 4A; Supplementary Fig. S4D). We also treated basal TICs with different *WNT5A* doses and found a consistent and dose-dependent decrease in spheroid size (Fig. 4B). Next, we isolated lineage⁻CD24^{high}CD49f^{low}CD61⁻ mature luminal cells (mLC) from WT and *Wnt5a*^{+/-} mice and cocultured them with basal or luminal TICs. mLCs did not form spheroid structure (Supplementary Fig. S4E, bottom). We found that coculturing basal TICs with WT mLC led to a significant reduction in mean size compared with basal TICs alone (Fig. 4C; Supplementary Fig. S4E). Coculturing with



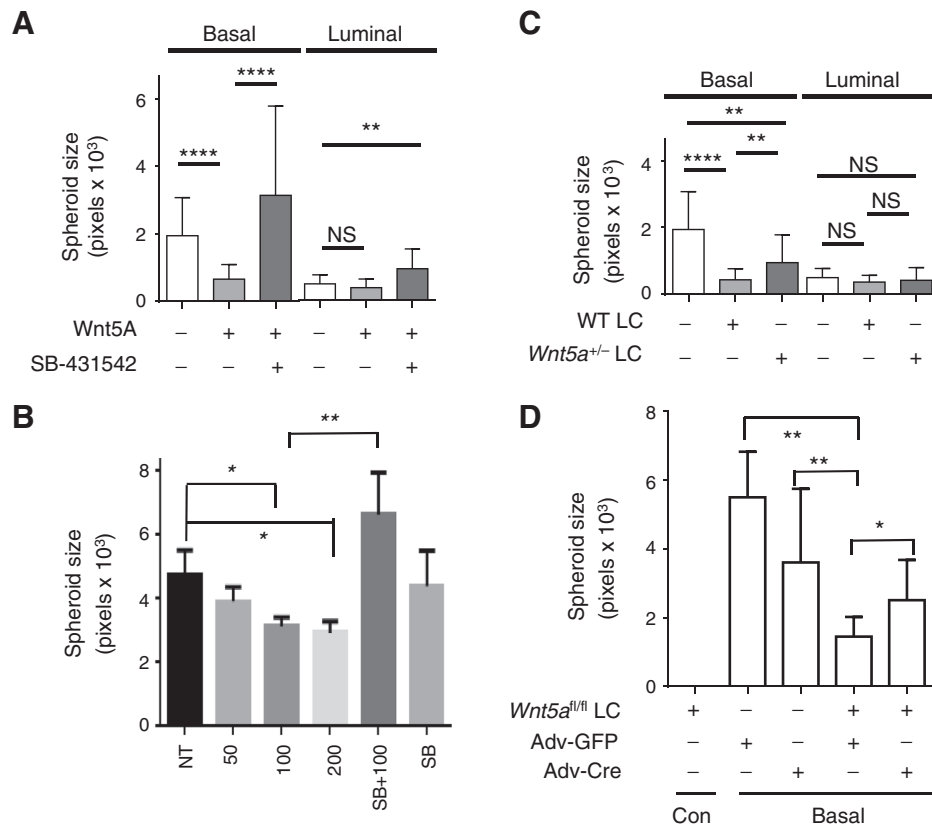
WT mLC had no impact on luminal TIC-formed spheroids (Fig. 4C; Supplementary Fig. S4E). Coculturing basal TICs with *Wnt5a*^{+/-} mLC partially restored spheroid size (Fig. 4C; Supplementary Fig. S4E). We confirmed that WT mLC secreted more WNT5A than *Wnt5a*^{+/-} mLC (Supplementary Fig. S2C). We also purified mLC from *Wnt5a*^{fl/fl} mice and cocultured these cells with basal TICs, either treated with adenovirus encoding GFP (Adv-GFP) or adenovirus encoding cre DNA recombinase (Adv-Cre) to deplete WNT5A expression (Supplementary Fig. S4F, right). We found mLC from *Wnt5a*^{fl/fl} mice did not form discernable spheroids (Fig. 4D; Supplementary Fig. S4F), similarly to mLC from WT mice (Supplementary Fig. S4E, bottom). Although Adv-GFP or Adv-Cre treatment had no significant influence on spheroid growth from basal TICs, coculturing with *Wnt5a*^{fl/fl} mLC significantly reduced spheroid size (Adv-GFP), which was reversed by the *Wnt5a* deletion with Adv-Cre treatment (Fig. 4D; Supplementary Fig. S4F). These data strongly suggest a specific paracrine signaling pathway mediated by WNT5A of luminal origin in suppressing basal TIC growth.

We stained frozen sections from basal TIC-formed spheroids and confirmed that basal TICs were able to form both hollow acinus-like structures as well as solid DCIS-like structures (Supplementary Fig. S4G; ref. 22). Most of spheroid cells are positive for luminal epithelial cell marker keratin 8 (KRT8), suggesting the differentiation from basal cells to luminal epithelial cells (Supplementary Fig. S4G). WNT5A was expressed by most of KRT8⁺ luminal cells and was low-to-absent from KRT8-negative cells (Supplementary Fig. S4G).

We also compared tumor onset days, multiplicity of tumors, and metastasis between *ErbB2*/WT and *ErbB2*/*Wnt5a*^{+/-} females. Our initial analysis of *Wnt5a*^{+/-} females showed no phenotype in mammary gland development based on whole mount (Supplementary Fig. S5A), H&E staining (Supplementary Fig. S5B), as well as the litter size and feeding. Heterozygous deletion of *Wnt5a* did not affect the primary tumor onset in the *ErbB2*-induced tumorigenesis (Fig. 5A). However, heterozygous *Wnt5a* deletion increased the tumor incidence (Fig. 5B). We also found that only 1 of 6 *ErbB2*/WT females had one small lung metastasis by histologic assessment, but 4 of 6 *ErbB2*/*Wnt5a*^{+/-} female mice had lung metastasis with numbers ranging from 2 to 19 (Fig. 5C and D).

WNT5A activates SMAD2 in a TGF β R-dependent manner

The TGF β -SMAD signaling pathway induces the expression WNT5A and in turn suppresses mammary morphogenesis and carcinogenesis (10, 15). We added a TGF β R1 kinase inhibitor SB-431542 together with WNT5A for spheroid growth, with the expectation that WNT5A could suppress spheroid growth when inhibiting TGF β -SMAD. Unexpectedly, we observed a significant size increase in basal TIC-formed spheroids compared with WNT5A alone (Fig. 4A and B; Supplementary Fig. S4D), suggesting that TGF β -SMAD is either parallel to or downstream of WNT5A. Luminal TIC-formed spheroids were not affected by WNT5A treatment, but inhibition of TGF β -SMAD significantly increased the mean size from luminal TICs (Fig. 4A; Supplementary Fig. S4D). SB-431542 alone had no significant impact on

**Figure 4.**

WNT5A suppresses the growth of basal TIC via a paracrine manner. A, basal and luminal TICs were purified from preneoplastic mammary glands of 5-month-old *MMTV-ErbB2* female mice and seeded onto Matrigel-coated chambers, either mock-treated or treated with 100 ng/mL of WNT5A alone or in combination with 5 μ mol/L of SB-431542. B, basal TICs were purified and seeded onto Matrigel-coated chambers, either nontreated (NT), treated with different doses of WNT5A (50, 100, or 200 ng/mL) or 100 ng/mL WNT5A + 5 μ mol/L SB-431542 (SB + 100) or 5 μ mol/L SB-431542 (SB). C, basal and luminal TICs were purified and seeded onto Matrigel, either alone or cocultured with purified mLCs from either WT or *WNT5A*^{+/-} female mice at 1:5 ratio. D, basal TICs (basal) and mLCs from *WNT5A*^{fl/fl} females (*WNT5A*^{fl/fl} LC) were cocultured onto Matrigel at 1:5 ratio; 24 hours later, cells were either treated with adenovirus encoding GFP (Adv-GFP) or Cre DNA recombinase (Adv-Cre). Basal TICs alone were also treated with Adv-GFP or Adv-Cre. *WNT5A*^{fl/fl} LC did not form spheroids under these conditions (*WNT5A*^{fl/fl} LC, first column). A–D, after 3 weeks, spheroids were photographed and their size in pixels was quantitated with ImageJ (*, $P < 0.05$; **, $P \leq 0.0042$; ****, $P < 0.0001$); mean \pm SEM; $n = 10$ –27 spheroids from two independent experiments).

spheroid size from basal TICs (Fig. 4B, comparing NT and SB). We purified primary basal cells and luminal cells from preneoplastic mouse mammary gland and confirmed the purity of basal or luminal cells by using KRT5 as a basal-specific marker and KRT8 as a luminal-specific marker (Fig. 6A). Basal epithelial cells had low level of phosphorylation of SMAD2 (p-SMAD2), whereas luminal cells had constitutively high p-SMAD2 (Fig. 6A). WNT5A induced p-SMAD2 in basal cells in a TGF β 1-dependent manner because SB-431542 inhibited WNT5A-induced p-SMAD2 (Fig. 6A). Luminal cells had higher basal level of p-SMAD2 that was not further induced by WNT5A; SB-431542 treatment, either alone or in combination with WNT5A treatment, did not significantly reduce p-SMAD2 signal (Fig. 6A). We did not observe p-SMAD3 (the lower 52 KD band in third panel, Fig. 6A). WNT5A was expressed stronger in luminal epithelial cells and significantly less in basal epithelial cells (Fig. 6A). We confirmed WNT5A-induced p-SMAD2 in HMLE cells (Supplementary Fig. S6A) and in MCF10A cells (Supplementary Fig. S6B), two immortalized human mammary epithelial lines. TGF β induced 4- to 5-fold higher p-SMAD2 than WNT5A in MCF10A cells (Supplementary Fig. S6B; Fig. 6B).

We found a similar but delayed WNT5A-induced p-SMAD2 and high basal level of p-SMAD3 in MDA-MB-231 cells, a breast cancer cell line (Supplementary Fig. S6C). We silenced TGF β 1 in MCF10A and found that downregulation of TGF β 1 reduced WNT5A- and TGF β -induced p-SMAD2 (Fig. 6B), and further confirmed the necessity of TGF β 1 kinase activity by two independent inhibitors SB-341542 and SB-505124 (Supplementary Fig. S6A and S6D). In addition, WNT5A significantly repressed the expression of cyclin D1 and β -catenin, whereas TGF β increased the expression of cell-cycle inhibitors p15 and p21 (Supplementary Fig. S6E). WNT5A and TGF β induced the repression of some common genes, including antiapoptotic *BCL-XL* and *GATA3* (Supplementary Fig. S6E), further supporting a specific yet different role of WNT5A compared with TGF β in mammary epithelial cells.

RYK is a coreceptor for WNT5A induced-SMAD2 activation

We examined the expression of WNT5A receptors and found that RYK mRNA was reduced in primary tumors within the TCGA breast cancer dataset when compared with normal tissues

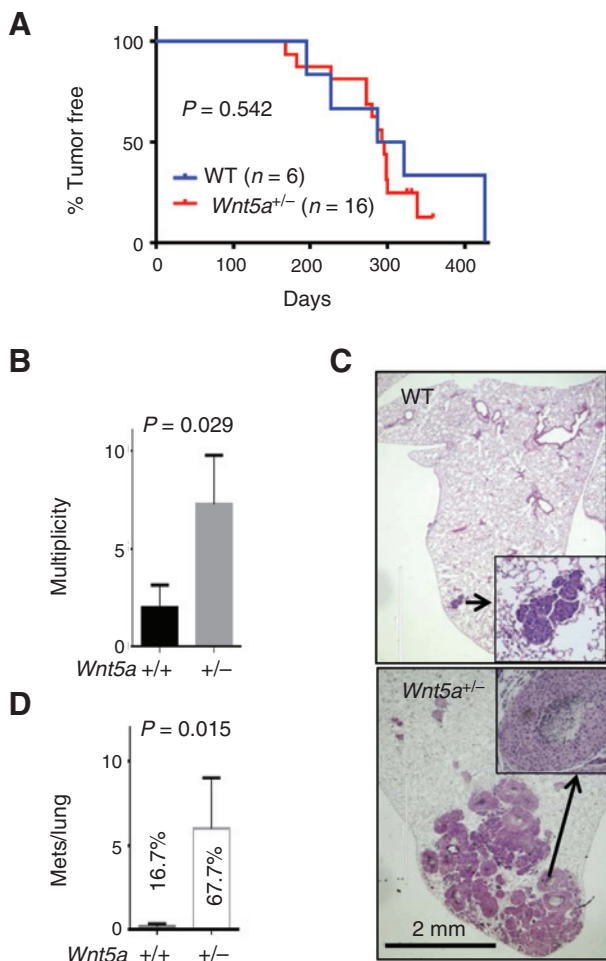


Figure 5. WNT5A inhibits tumor multiplicity and metastasis in ErbB2-induced mammary cancer. MMTV-*ErbB2* transgenic mice were crossed with *WNT5A*^{+/-} to produce *ErbB2*/WT and *ErbB2*/*WNT5A*^{+/-} mice. Tumor onset days (A), multiplicity (B), as well as lung metastasis assessed by H&E staining of paraffin-embedded lung sections (representative images in C and summarized in D) were assessed. The percentage in C indicates the percentage of animals with lung metastasis. Numbers of metastatic nodules were plotted and *P* values indicated. A, *n* = 6 for *ErbB2*/WT and *n* = 16 for *ErbB2*/*WNT5A*^{+/-}; B and D, *n* = 6 for each group.

(Supplementary Fig. S7A). The reduction of *RYK* mRNA was seen across all four subtypes (Supplementary Fig. S7B). The differential expression of WNT5A receptors from luminal and basal cells were examined using the GSE37223 dataset (30). *RYK* mRNA was 1.76-fold higher in basal cells than in luminal cells (Supplementary Fig. S7C). We confirmed higher *RYK* expression in KRT8-negative basal cells from human mammary ducts relative to KRT8-positive luminal cells (Supplementary Fig. S7D), and observed a significantly loss of *RYK* expression in adjacent invasive cancer cells (Supplementary Fig. S7D). We also found that mouse primary basal cells had higher *RYK* expression relative to luminal cells (Fig. 6A). *ROR1* mRNA was 4-fold higher in basal cells than in luminal cells (Supplementary Fig. S7C). We failed to detect *ROR1* protein (data not shown), confirming its nature as a fetal antigen (21). Both *ROR2* and *FZD4* did not possess significant difference

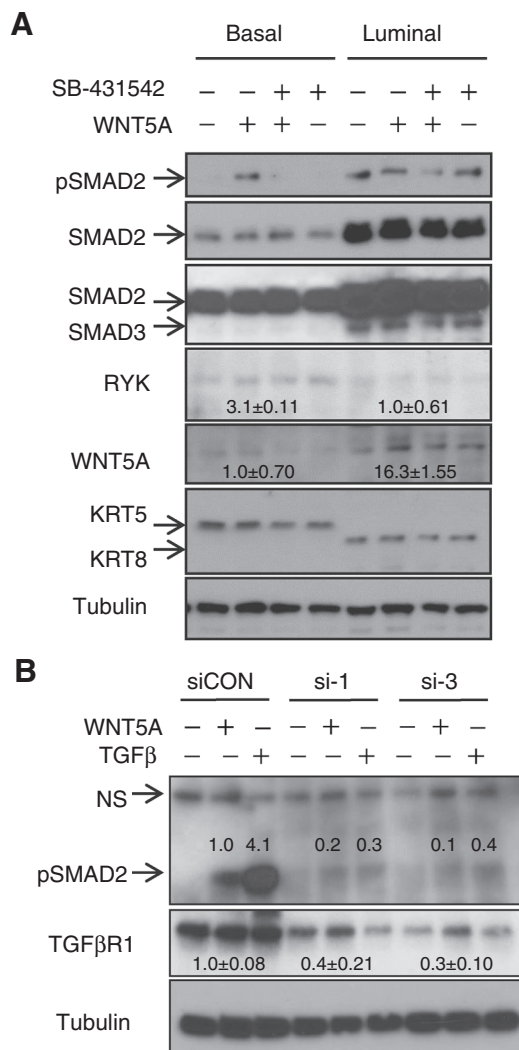
between luminal and basal cells (Supplementary Fig. S7C; ref. 17). As nonrelevant FZD members that mediate classical Wnt signaling, *FZD6*, but not *FZD5*, was found to be elevated in basal cells relative to luminal cells (Supplementary Fig. S7C), supporting the role of paracrine classic Wnt signaling in mammary epithelium (32, 33).

We designed two shRNAs that significantly reduced *RYK* expression to about 10% relative to MCF10A cells expressing a luciferase-targeting control shRNA (Fig. 7A). WNT5A induced p-SMAD2 that was lower than TGF β -induced p-SMAD2 (Fig. 7A). Silencing *RYK* in MCF10A cells led to a significantly reduced p-SMAD2 induced by WNT5A, and to a lesser extent the TGF β -induced p-SMAD2, relative to parental MCF10A cells (Supplementary Fig. S8A) or MCF10A cells expressing control shRNA (Fig. 7A and quantitated in Fig. 7B). Interestingly, *RYK* silencing led to significant increase of TGF β R1 (Fig. 7A) and SMAD2/3 (Fig. 7A; Supplementary Fig. S8A), supporting a potential negative feedback from *RYK* to SMAD and TGF β R1. We further confirmed a dose-dependent increase of p-SMAD2 in response to WNT5A ranging from 0 to 200 ng/mL, which agrees with the dose-dependent suppression of spheroid size (Fig. 4B) and was dependent on *RYK* expression (Fig. 7C). Interestingly, *RYK* deficiency led to a significant JNK activation at both basal and WNT5A-induced levels (Fig. 7C). These results suggest that *RYK* preferentially binds to WNT5A to activate p-SMAD2 and *RYK* deficiency leads to other WNT5A receptor-mediated signaling pathways as recently reported (37). Mechanistically, we found a constitutive interaction between TGF β R1 and *RYK* that was further enhanced by WNT5A treatment (Fig. 7D); however, TGF β treatment released *RYK* protein from the TGF β R complex (Fig. 7D). Anti-*RYK* antibody failed to pull down TGF β R (data not shown), possibly due to competitive binding to the similar sites on *RYK*.

Consistently, *RYK* deficiency in MCF10A cells increased spheroid size and led to an invasive phenotype (Supplementary Fig. S8B and S8C). We analyzed a published GEO dataset GSE2034, including 255 clinical breast cancer specimens. We equally separated the 255 specimens into 4 groups based on the expression of *RYK* (Supplementary Fig. S8D) or *SMAD2* (Supplementary Fig. S8E), or interaction between *RYK* and *SMAD2* (Supplementary Fig. S8F; Fig. 7E). The expression of either *RYK* or *SMAD2* was not correlated with metastasis-free survival (MFS; Supplementary Fig. S8D and S8E). We found that patients whose specimens have high expression of both *RYK* and *SMAD2* had the longest time to MFS and those whose specimens have low *RYK* and *SMAD2* had the shortest MFS (Supplementary Fig. S8F; Fig. 7E, *P* = 0.006, comparing groups 1/1 with 0/0). This result suggests the functional interaction between *RYK* and *SMAD2* to suppress the progression and metastasis of human cancer.

Discussion

It is essential for cancer biology and therapy to understand how cancer initiates and how TICs evade the normal suppressive microenvironment. Here, we uncover an important paracrine regulation from luminal cell-produced WNT5A, in a TGF β R-dependent manner (10), to suppress the growth of basal TICs, thus tumorigenesis (Supplementary Fig. S9). WNT5A induces a specific activation of TGF β R/SMAD2 module in basal cells to suppress their growth. *RYK*, one of the WNT5A receptors, forms a complex with TGF β R1 upon WNT5A induction and in turn leads to the phosphorylation and activation of SMAD2 (Supplementary

**Figure 6.**

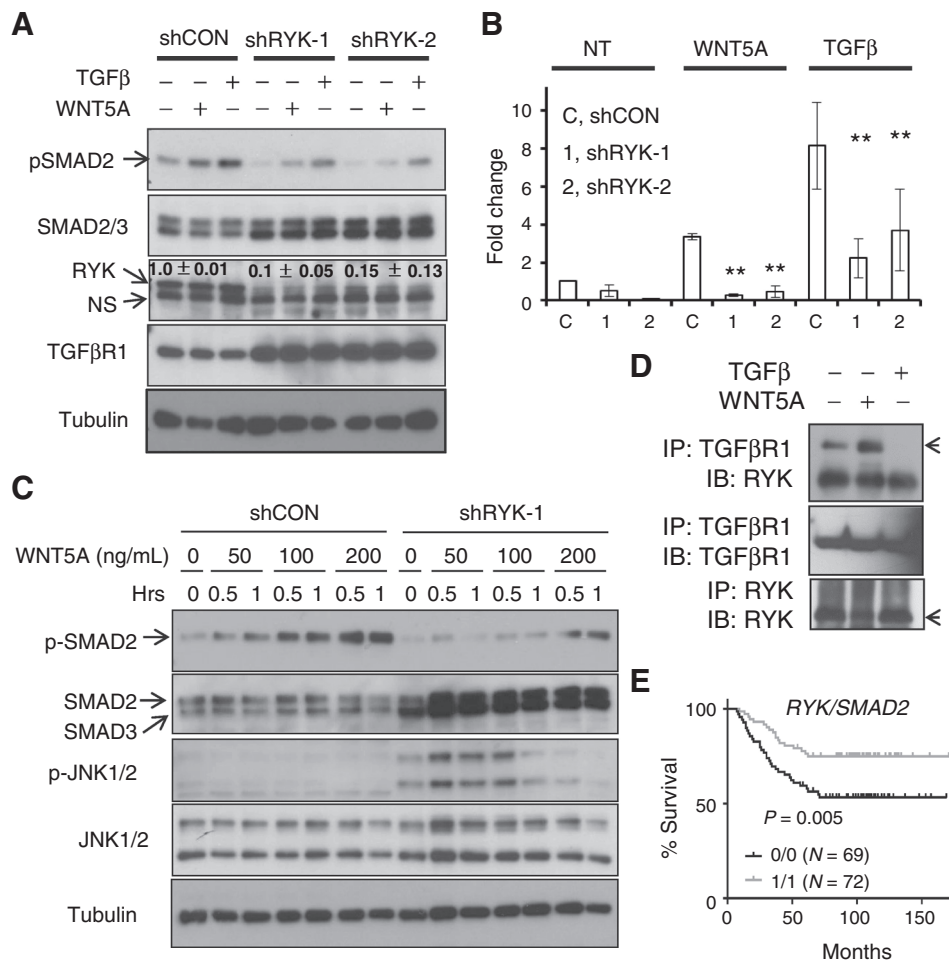
WNT5A induces the phosphorylation of SMAD2 in a TGFβ receptor-dependent fashion. A, basal and luminal mammary epithelial cells were purified from preneoplastic mammary gland of 5-month-old *ErbB2/WNT5A*^{+/-} mice and cultured in 24-well plates for 72 hours. Cells were either mock-treated, treated with WNT5A (100 ng/mL), WNT5A+SB-431542 (5 μmol/L), or SB-431542 alone for 1 hour. B, MCF10A cells were transiently transfected with control siRNA (siCON), or two independent siRNAs to TGFβR1 (si-1 and si-3). Ninety-six hours later, cells were either treated with WNT5A (100 ng/mL) or TGFβ (5 ng/mL) for 1 hour. For A-B, cell lysates were collected, separated by SDS-PAGE, and immunoblotted with the indicated antibodies (*n* = 2-3). Band densitometry was measured by ImageJ.

Fig. S9). This unique signaling pathway is important for the growth of basal TICs during ErbB2-induced breast cancer.

WNT5A is a downstream effector of TGFβ and mediates the suppressive effect of TGFβ on mammary morphogenesis and carcinogenesis (10, 15). Our study identified a feed-forward activation pathway that TGFβ induces WNT5A within luminal cells and WNT5A further expands the TGFβR/SMAD signaling in basal cells, for example, basal TIC in the case of breast cancer model, to suppress their growth. It is known that normal tissue microenvironment suppresses uncontrolled proliferation of

stem cells and promotes their asymmetrical proliferation (38). Mammary stem cells are known to proliferate during pregnancy and diestrus stage of estrus cycle mediated by classical Wnt signaling and receptor activator for NF-κB ligand (RANKL), a process activated by luminal progesterone signaling (32, 33). Coincidentally, both classic Wnt signaling (39) and RANKL (40, 41) are critical to promote carcinogen- or oncogene-induced mammary cancer, although the connection between the expansion of mammary stem cells and cancer promotion is difficult to prove and yet to be established. WNT5A, on the other hand, likely serves a "niche" component to counterbalance classical Wnt or RANKL effects on the expansion of mammary stem cells, that is, the basal TICs, and thus suppresses tumorigenesis. WNT5A plays a broader role in tissue stem cells and its ablation increases proliferative intestinal stem cells (27). WNT5A functions as a negative regulator of self-renewal or proliferation in embryonic and hematopoietic stem cells (42, 43) through RYK (44). Interestingly, in colon WNT5A induces p-SMAD3 not p-SMAD2 in a ROR1/2-dependent manner, suggesting that WNT5A uses a similar mechanism to regulate the homeostasis of tissue stem cells. Among many WNT5A receptors, RYK is highly expressed in normal mammary tissue and decreased in all breast cancer subtypes (Supplementary Fig. S7B). Our analysis of the Affymetrix array dataset GSE2034 based on 255 human breast cancer specimens further corroborates the role of RYK in suppressing metastasis in conjunction with SMAD2 (Fig. 7E). A recent study showed that WNT5A promotes mammosphere growth via ROR2-mediated JNK activation (37). One potential explanation is that WNT5A preferentially interacts with RYK; in the absence of RYK, WNT5A activates JNK1/2 (Fig. 7C) in an ROR2-dependent manner (37). It is known that WNT5A induces RANKL expression via ROR2-mediated JNK activation during osteoclastogenesis (45), a potential mechanism that might take place in mammary epithelium, when condition permits, to promote mammary stem cells. Another potential explanation is that we used mammary epithelial cells from preneoplastic *MMTV-ErbB2* female mice. ErbB2 promotes strong activation of the MAPK Erk1/2 pathway for mammary tumorigenesis, thus surpasses the necessity of JNK activation as seen in normal mammary epithelial cells or those from *MMTV-Wnt1* transgenic mice (37). Indeed, genetic deletion of JNK in mammary epithelial cells led to increased ductal morphogenesis and mammary tumorigenesis, suggesting its tumor suppressive role in mammary cancer (46).

The paracrine interactions between basal and luminal compartments within the mammary epithelium have broader implications. We reported here that WNT5A is highly expressed in luminal cells and inhibits the growth of basal TICs, which likely needs to evade the WNT5A-mediated or other suppressive microenvironment signals during the oncogenic process. We believe that basal TICs have to undergo luminal differentiation during ErbB2-induced mammary tumorigenesis because all ErbB2-induced tumors express luminal keratins (22). During the basal to luminal differentiation, WNT5A perceivably loses its control on tumor cells as evidenced by the fact that WNT5A failed to induce further p-SMAD2 in ErbB2⁺ luminal cells (Fig. 6A). It is known that Notch activation leads to the commitment of mammary stem cells to luminal differentiation during Notch-induced tumorigenesis (47). ErbB2 may have a similar function as Notch to initiate tumors from mammary stem cells.

**Figure 7.**

RYK is the coreceptor for WNT5A-induced activation of SMAD2. A and B, MCF10A cells were infected with lentiviral particles encoding control luciferase shRNA (shCON) or two independent *RYK* shRNAs with coexpression of GFP. GFP-positive cells were collected by flow cytometry. Parental MCF10A (data not shown here), MCF10A cells with control shRNA, or cells with *RYK* shRNA1 or shRNA2 were cultured and either left untreated (NT) or treated with WNT5A (100 ng/mL) or TGFβ (5 ng/mL). Cell lysates were collected, separated by SDS-PAGE, and immunoblotted with the indicated antibodies. Representative images are shown in A and quantitated in B; $P < 0.01$; $n = 3$. C, MCF10A cells with control shRNA or cells with *RYK* shRNA1 were treated with different amount of WNT5A as indicated for 0.5 or 1 hour. Cell lysates were collected, followed by immunoblotting with the indicated antibodies. D, MCF10A cells were treated with WNT5A (100 ng/mL) or TGFβ1 (5 ng/mL) for 1 hour. Cells were lysed and lysates were immunoprecipitated with anti-*RYK* and anti-TGFβR1 antibodies. Immunocomplex was resolved by SDS-PAGE, followed by immunoblotting with the indicated antibodies. E, the Affymetrix GEO dataset GSE2034 containing 255 human breast cancer specimens with supplemented clinical records was downloaded. Two hundred and fifty-five specimens in GSE2034 were separated into four groups based on the expression level of *RYK* and *SMAD2*. Low (assigned as 0) and high (assigned as 1) expression of *RYK* or *SMAD2* were defined as expression values lower or higher than median values; *N*, numbers; a *P* value comparing 1/1 group versus 0/0 group is indicated. The correlation between MFS and *RYK/SMAD2* expression was analyzed and Kaplan-Meier curve was graphed using Prism 6 software.

Disclosure of Potential Conflicts of Interest

No potential conflicts of interest were disclosed.

Authors' Contributions

Conception and design: N. Borcherding, D. Kusner, R. Kolb, W. Zhang
Development of methodology: N. Borcherding, D. Kusner, R. Kolb, W. Li, W. Zhang
Acquisition of data (provided animals, acquired and managed patients, provided facilities, etc.): N. Borcherding, D. Kusner, R. Kolb, F. Yuan, R. Askeland, R.J. Weigel, W. Zhang
Analysis and interpretation of data (e.g., statistical analysis, biostatistics, computational analysis): N. Borcherding, D. Kusner, R. Kolb, Q. Xie, F. Yuan, G. Velez, R.J. Weigel, W. Zhang

Writing, review, and/or revision of the manuscript: N. Borcherding, D. Kusner, R. Kolb, R. Askeland, R.J. Weigel, W. Zhang

Administrative, technical, or material support (i.e., reporting or organizing data, constructing databases): N. Borcherding, Q. Xie, W. Li, R.J. Weigel
Study supervision: W. Zhang

Acknowledgments

The authors thank Dr. Terry Yamaguchi from the National Cancer Institute for providing the *Wnt5a^{fl/fl}* mice; the authors thank Drs. Hasem Habelhah and Dawn Quelle for technical support and insights; the authors thank Dr. Songhai Chen for providing frozen tissues of human breast cancer; and thank Genetex and Santa Cruz Biotechnology for providing important antibodies.

Grant Support

This work was supported by NIH grant K99/R00 CA158055 (W. Zhang), NIH T32 GM007337 (N. Borcherdig and G. Velez), NIH T32 AI007260 (R. Kolb), and a V Scholar award from the V Research Foundation for the Cancer (W. Zhang). The authors were supported by a Department Startup grant and Seed grant from the Department of Pathology and a Breast Cancer Research Grant for Holden Comprehensive Cancer Center, University of Iowa Carver College of Medicine (W. Zhang). This work was benefited from the National Cancer Institute of the NIH under Award Number P30CA086862. Research reported in this publication was supported by the National Center for Research

Resources of the NIH under Award Number 1S10 RR027219. Finally, these results here are in whole or part based upon data generated by the TCGA Research Network (<http://cancergenome.nih.gov/>).

The costs of publication of this article were defrayed in part by the payment of page charges. This article must therefore be hereby marked advertisement in accordance with 18 U.S.C. Section 1734 solely to indicate this fact.

Received September 17, 2014; revised February 20, 2015; accepted March 9, 2015; published OnlineFirst March 13, 2015.

References

- Taipale J, Beachy PA. The Hedgehog and Wnt signalling pathways in cancer. *Nature* 2001;411:349–54.
- Habas R, Dawid IB, He X. Coactivation of Rac and Rho by Wnt/Frizzled signaling is required for vertebrate gastrulation. *Genes Dev* 2003;17:295–309.
- Wansleeben C, Meijlink F. The planar cell polarity pathway in vertebrate development. *Dev Dynamics* 2011;240:616–26.
- Slusarski DC, Yang-Snyder J, Busa WB, Moon RT. Modulation of embryonic intracellular Ca²⁺-signaling by Wnt-5A. *Dev Biol* 1997;182:114–20.
- Westfall TA, Brimeyer R, Twedt J, Gladon J, Olberding A, Furutani-Seiki M, et al. Wnt-5/pipetail functions in vertebrate axis formation as a negative regulator of Wnt/ β -catenin activity. *J Cell Biol* 2003;162:889–98.
- Anastas JN, Moon RT. WNT signalling pathways as therapeutic targets in cancer. *Nat Rev Cancer* 2013;13:11–26.
- Yuzugullu H, Benhaj K, Ozturk N, Senturk S, Celik E, Toylyu A, et al. Canonical Wnt signaling is antagonized by noncanonical Wnt5a in hepatocellular carcinoma cells. *Mol Cancer* 2009;8:90.
- Liang H, Chen Q, Coles AH, Anderson SJ, Pihan G, Bradley A, et al. Wnt5a inhibits B cell proliferation and functions as a tumor suppressor in hematopoietic tissue. *Cancer Cell* 2003;4:349–60.
- Ying J, Li H, Yu J, Ng KM, Poon FF, Wong SCC, et al. WNT5A exhibits tumor-suppressive activity through antagonizing the Wnt/ β -catenin signaling, and is frequently methylated in colorectal cancer. *Clin Cancer Res* 2008;14:55–61.
- Roarty K, Baxley SE, Crowley MR, Frost AR, Serra R. Loss of TGF- β or Wnt5a results in an increase in Wnt/ β -catenin activity and redirects mammary tumour phenotype. *Breast Cancer Res* 2009;11:R19.
- Bitler BG, Nicodemus JP, Li H, Cai Q, Wu H, Hua X, et al. Wnt5a suppresses epithelial ovarian cancer by promoting cellular senescence. *Cancer Res* 2011;71:6184–94.
- Lejeune S, Huguet EL, Hamby A, Poulson R, Harris AL. Wnt5a cloning, expression, and up-regulation in human primary breast cancers. *Clin Cancer Res* 1995;1:215–22.
- Jönsson M, Dejmeck J, Bendahl P-O, Andersson T. Loss of Wnt-5a protein is associated with early relapse in invasive ductal breast carcinomas. *Cancer Res* 2002;62:409–16.
- Leris ACA, Roberts TR, Jiang WG, Newbold RF, Mokbel K. WNT5A expression in human breast cancer. *Anticancer Res* 2005;25:731–34.
- Roarty K, Serra R. Wnt5a is required for proper mammary gland development and TGF- β -mediated inhibition of ductal growth. *Development* 2007;134:3929–39.
- Keeble TR, Halford MM, Seaman C, Kee N, Macheda M, Anderson RB, et al. The Wnt receptor Ryk is required for Wnt5a-mediated axon guidance on the contralateral side of the corpus callosum. *J Neurosci* 2006;26:5840–48.
- Mikels AJ, Nusse R. Purified Wnt5a protein activates or inhibits β -catenin-TCF signaling depending on receptor context. *PLoS Biol* 2006;4:e115.
- Fukuda T, Chen L, Endo T, Tang L, Lu D, Castro JE, et al. Antisera induced by infusions of autologous Ad-CD154-leukemia b cells identify ROR1 as an oncofetal antigen and receptor for Wnt5a. *Proc Natl Acad Sci U S A* 2008;105:3047–52.
- Hovens CM, Stacker SA, Andres AC, Harpur AG, Ziemiecki A, Wilks AF. RYK, a receptor tyrosine kinase-related molecule with unusual kinase domain motifs. *Proc Natl Acad Sci U S A* 1992;89:11818–22.
- Katso RMT, Manek S, Ganjavi H, Biddolph S, Charnock MFL, Bradburn M, et al. Overexpression of H-Ryk in epithelial ovarian cancer: prognostic significance of receptor expression. *Clin Cancer Res* 2000;6:3271–81.
- Borcherdig N, Kusner D, Liu GH, Zhang W. ROR1, an embryonic protein with an emerging role in cancer biology. *Protein & Cell* 2014;5:496–502.
- Zhang W, Tan W, Wu X, Poustovoitov M, Strasner A, Li W, et al. A NIK-IKK α module expands ErbB2-induced tumor-initiating cells by stimulating nuclear export of p27/Kip1. *Cancer Cell* 2013;23:647–59.
- Zhu J, Sanborn JZ, Benz S, Szeto C, Hsu F, Kuhn RM, et al. The UCSC cancer genomics browser. *Nat Meth* 2009;6:239–40.
- Debnath J, Muthuswamy SK, Brugge JS. Morphogenesis and oncogenesis of MCF-10A mammary epithelial acini grown in three-dimensional basement membrane cultures. *Methods* 2003;30:256–68.
- Schneider CA, Rasband WS, Eliceiri KW. NIH Image to ImageJ: 25 years of image analysis. *Nat Meth* 2012;9:671–75.
- Zhang W, Kater AP, Widhopf GF, Chuang H-Y, Enzler T, James DF, et al. B-cell activating factor and v-Myc myelocytomatosis viral oncogene homolog (c-Myc) influence progression of chronic lymphocytic leukemia. *Proc Natl Acad Sci U S A* 2010;107:18956–60.
- Miyoshi H, Ajima R, Luo CT, Yamaguchi TP, Stappenbeck TS. Wnt5a potentiates TGF- β signaling to promote colonic crypt regeneration after tissue injury. *Science* 2012;338:108–13.
- Muller WJ, Sinn E, Pattengale PK, Wallace R, Leder P. Single-step induction of mammary adenocarcinoma in transgenic mice bearing the activated c-neu oncogene. *Cell* 1988;54:105–15.
- Yamaguchi TP, Bradley A, McMahon AP, Jones S. A Wnt5a pathway underlies outgrowth of multiple structures in the vertebrate embryo. *Development* 1999;126:1211–23.
- Kannan N, Huda N, Tu L, Droumeva R, Aubert G, Chavez E, et al. The luminal progenitor compartment of the normal human mammary gland constitutes a unique site of telomere dysfunction. *Stem Cell Rep* 2013;1:28–37.
- Subramanian A, Tamayo P, Mootha VK, Mukherjee S, Ebert BL, Gillette MA, et al. Gene set enrichment analysis: a knowledge-based approach for interpreting genome-wide expression profiles. *Proc Natl Acad Sci U S A* 2005;102:15545–50.
- Asselin-Labat ML, Vaillant F, Sheridan JM, Pal B, Wu D, Simpson ER, et al. Control of mammary stem cell function by steroid hormone signalling. *Nature* 2010;465:798–802.
- Joshi PA, Jackson HW, Beristain AG, Di Grappa MA, Mote PA, Clarke CL, et al. Progesterone induces adult mammary stem cell expansion. *Nature* 2010;465:803–7.
- Dontu G, Abdallah WM, Foley JM, Jackson KW, Clarke MF, Kawamura MJ, et al. *In vitro* propagation and transcriptional profiling of human mammary stem/progenitor cells. *Genes Dev* 2003;17:1253–70.
- Pastrana E, Silva-Vargas V, Doetsch F. Eyes wide open: a critical review of sphere-formation as an assay for stem cells. *Cell Stem Cell* 2011;8:486–98.
- Debnath J, Brugge JS. Modelling glandular epithelial cancers in three-dimensional cultures. *Nat Rev Cancer* 2005;5:675–88.
- Many AM, Brown AMC. Both canonical and non-canonical wnt signaling independently promote stem cell growth in mammospheres. *PLoS ONE* 2014;9:e101800.
- Blanpain C, Fuchs E. Stem cell plasticity. Plasticity of epithelial stem cells in tissue regeneration. *Science* 2014;344:1242281.
- Shackleford GM, MacArthur CA, Kwan HC, Varmus HE. Mouse mammary tumor virus infection accelerates mammary carcinogenesis in Wnt-1 transgenic mice by insertional activation of int-2/Fgf-3 and hst/Fgf-4. *Proc Natl Acad Sci U S A* 1993;90:740–4.

Borcherding et al.

40. Tan W, Zhang W, Strasner A, Grivennikov S, Cheng JQ, Hoffman RM, et al. Tumour-infiltrating regulatory T cells stimulate mammary cancer metastasis through RANKL-RANK signalling. *Nature* 2011;470:548–53.
41. Schramek D, Leibbrandt A, Sigl V, Kenner L, Pospisilik JA, Lee HJ, et al. Osteoclast differentiation factor RANKL controls development of progesterone-driven mammary cancer. *Nature* 2010;468:98–102.
42. Nemeth MJ, Topol L, Anderson SM, Yang Y, Bodine DM. Wnt5a inhibits canonical Wnt signaling in hematopoietic stem cells and enhances repopulation. *Proc Natl Acad Sci U S A* 2007;104:15436–41.
43. Hwang Y-S, Chung BG, Ortmann D, Hattori N, Moeller H-C, Khademhosseini A. Microwell-mediated control of embryoid body size regulates embryonic stem cell fate via differential expression of WNT5a and WNT11. *Proc Natl Acad Sci U S A* 2009;106:16978–83.
44. Povinelli BJ, Nemeth MJ. Wnt5a regulates hematopoietic stem cell proliferation and repopulation through the Ryk receptor. *Stem Cells* 2014;32:105–15.
45. Maeda K, Kobayashi Y, Udagawa N, Uehara S, Ishihara A, Mizoguchi T, et al. Wnt5a-Ror2 signaling between osteoblast-lineage cells and osteoclast precursors enhances osteoclastogenesis. *Nature Medicine* 2012;18:405–12.
46. Chen P, O'Neal JF, Ebel ND, Cantrell MA, Mitra S, Nasrazadani A, et al. Jnk2 effects on tumor development, genetic instability and replicative stress in an oncogene-driven mouse mammary tumor model. *PLoS ONE* 2010;5:e10443.
47. Bouras T, Pal B, Vaillant F, Harburg G, Asselin-Labat ML, Oakes SR, et al. Notch signaling regulates mammary stem cell function and luminal cell-fate commitment. *Cell Stem Cell* 2008;3:429–41.

Cancer Research

The Journal of Cancer Research (1916–1930) | The American Journal of Cancer (1931–1940)

Paracrine WNT5A Signaling Inhibits Expansion of Tumor-Initiating Cells

Nicholas Borchering, David Kusner, Ryan Kolb, et al.

Cancer Res 2015;75:1972-1982. Published OnlineFirst March 13, 2015.

Updated version	Access the most recent version of this article at: doi: 10.1158/0008-5472.CAN-14-2761
Supplementary Material	Access the most recent supplemental material at: http://cancerres.aacrjournals.org/content/suppl/2015/03/12/0008-5472.CAN-14-2761.DC1

Cited articles	This article cites 46 articles, 21 of which you can access for free at: http://cancerres.aacrjournals.org/content/75/10/1972.full#ref-list-1
Citing articles	This article has been cited by 2 HighWire-hosted articles. Access the articles at: http://cancerres.aacrjournals.org/content/75/10/1972.full#related-urls

E-mail alerts	Sign up to receive free email-alerts related to this article or journal.
Reprints and Subscriptions	To order reprints of this article or to subscribe to the journal, contact the AACR Publications Department at pubs@aacr.org .
Permissions	To request permission to re-use all or part of this article, use this link http://cancerres.aacrjournals.org/content/75/10/1972 . Click on "Request Permissions" which will take you to the Copyright Clearance Center's (CCC) Rightslink site.